NANO · MICRO small
www.small-journal.com

Graphene Oxide-Assisted and DNA-Modulated SERS of AuCu Alloy for the Fabrication of Apurinic/Apyrimidinic Endonuclease 1 Biosensor

Junyao Li, Hang Heng, Jianlin Lv, Tingting Jiang, Zhaoyin Wang, and Zhihui Dai**

Fabrication of high-performance surface-enhanced Raman scattering (SERS) biosensors relies on the coordination of SERS substrates and sensing strategies. Herein, a SERS active AuCu alloy with a starfish-like structure is prepared using a surfactant-free method. By covering the anisotropic AuCu alloy with graphene oxide (GO), enhanced SERS activity is obtained owing to graphene-enhanced Raman scattering and assembly of Raman reporters. Besides, stability of SERS is promoted based on the protection of GO to the AuCu alloy. Meanwhile, it is found that SERS activity of AuCu/GO can be regulated by DNA. The regulation is sequence and length dual-dependent, and short polyT reveals the strongest ability of enhancing the SERS activity. Relying on this phenomenon, a SERS biosensor is designed to quantify apurinic/apyrimidinic endonuclease 1 (APE1). Because of the APE1-induced cycling amplification, the biosensor is able to detect APE1 sensitively and selectively. In addition, APE1 in human serum is analyzed by the SERS biosensor and enzyme-linked immunosorbent assay (ELISA). The data from the SERS method are superior to that from ELISA, indicating great potential of this biosensor in clinical applications.

Since the intensity of Raman scattering can be dramatically improved,[1] surface-enhanced Raman scattering (SERS) has been developed to be a sensitive method for the fabrication of biosensors.[2] Typically, SERS is achieved by metallic nanomaterials due to chemical and electromagnetic effects.[3] In particular, metallic nanomaterials with anisotropic structures exhibit stronger SERS activity, because they provide edges and tips that are enhanced electromagnetic fields called hot spots.[4] Currently, several anisotropic metallic nanomaterials including nanorods,[5] nanoplates,[6] nanocubes,[7] nanocages,[8] and branched nanoparticles–nanostars[9] have been obtained and chosen as substrates of SERS assays.[10] Besides, composition of metallic nanomaterials is crucial to their SERS performances.[11] In comparison with nanomaterials containing one metal element, alloy is more likely to perform better in SERS.[12] For example, gold–silver (AuAg) alloy reveals larger SERS activity than pure Au nanomaterials.[13] To our knowledge, Au,[14] Ag, and copper (Cu) are candidates to form SERS substrates.[13c] Among them, Au is chemical stability,[15] but relatively poor in enhancing SERS activity. Ag is vulnerable to surface oxidation, thus limiting its applications in SERS assays.[16] In consideration of stability and promotion of SERS, AuCu alloy is an ideal substrate, especially if the AuCu alloy possesses anisotropic structure and can be prepared using an environment-friendly method.

Graphene, a famous carbon material,[17] attracts the attention for graphene-enhanced Raman scattering (GERS).[18] Hot spots created by metallic nanomaterials on one side of graphene can pass through graphene, thus improving Raman signal of absorbed molecules on the other side of graphene.[19] Graphene oxide (GO) is structurally similar to graphene,[20] but exhibits better solubility for plenty of groups on its surface.[21] For the following reasons, we believe GO can also enhance Raman scattering like graphene, thereby facilitating the design of SERS biosensors. First, groups on the surface of GO can serve as anchors to attach metallic nanomaterials.[22] Meanwhile, electrostatic attraction between GO and metallic nanomaterials is much stronger than that between graphene and metallic nanomaterials.[23] Accordingly, GO may avoid the aggregation of metallic nanomaterials, thus regulating the distribution and promoting stability of metallic nanomaterials (in particular surfactant-free metallic nanomaterials).[24] As a result, Raman scattering may be enhanced and stabilized. Second, heterocyclic aromatic compounds, such as methylene blue (MB), are typical Raman reporters, and are apt to be absorbed onto GO. Therefore, scattering of Raman reporters is remarkably promoted with the participation of GO. Third, it has been well known that GO can absorb DNA by π–π stacking.[25] By coordinating the effects of GO and DNA on SERS, novel strategies may be proposed to fabricate bioanalytical methods.

As a type of biomolecule with recognition capability, DNA has been employed to fabricate various SERS biosensors.[26] For

J. Li, J. Lv, T. Jiang, Dr. Z. Wang, Prof. Z. Dai
Jiangsu Key Laboratory of Biofunctional Materials
College of Chemistry and Materials Science
Nanjing Normal University
Nanjing 210023, P. R. China
E-mail: zywang@njnu.edu.cn; daizhihuii@njnu.edu.cn
H. Heng, Prof. Z. Dai
Center for Analysis and Testing
Nanjing Normal University
Nanjing 210023, P. R. China
The ORCID identification number(s) for the author(s) of this article can be found under https://doi.org/10.1002/smll.201901506.

DOI: 10.1002/smll.201901506

example, a SERS platform for DNA analysis is constructed by monitoring the change of DNA conformation on the surface of Au nanoparticles (AuNPs).[27] However, the function of DNA in current SERS biosensors is quite straightforward. In general, DNA induces aggregation of metallic nanomaterials, thereby increasing the signal of Raman reporters.[28] Actually, DNA can be absorbed on the surface of metallic nanomaterials by the interaction between bases and metal ions. Different bases have distinct affinities with the same metal ions. As to AuNPs, the absorption affinity varies in an order of T < C < G < A.[29] Meanwhile, relying on the interactions between bases and metal ions,[30] DNA with specific sequences can prepare metallic nanomaterials as templates.[31] Besides, it has been reported that DNA can guide the formation of anisotropic metallic nanomaterials by adding DNA to seed solution.[32] All of the above studies indicate that DNA may directly affect SERS activity of metallic nanomaterials. Therefore, by uncovering the intrinsic effect of DNA on SERS, more SERS biosensor can be designed based on novel principles, and the performances of related biosensors may be improved as well.

In this work, we put forward a simple method of synthesizing AuCu alloy with a starfish-like structure. Because of the anisotropic structure, the AuCu alloy can greatly enhance Raman signal of MB. AuCu alloy can combine with GO by electrostatic attraction, and the obtained AuCu/GO exhibits higher SERS activity. Taking AuCu/GO as a substrate, effect of DNA on SERS is further investigated. In comparison with purine bases (A and G), pyrimidine bases (T and C) are capable to enhance the SERS activity of AuCu/GO. Meanwhile, it is found that the SERS activity of AuCu alloy will decrease with the increase of DNA length. Obviously, effect of DNA on SERS of AuCu/GO is sequence and length dual-dependent. Relying on this principle, an excellent SERS biosensor has been designed to detect apurinic/apyrimidinic endonuclease 1 (APE1). APE1 in serum can be quantified with our proposed method, and the analytical performances of this method are superior to those of enzyme-linked immunosorbent assay (ELISA).

By integrating high-performance substrate with cycling amplification, we design a novel biosensor for the detection of APE1 (**Scheme 1**). First, AuCu alloy with a starfish-like structure is synthesized by directly reducing $HAuCl_4$ and $CuCl_2$ with L-ascorbic acid (AA). Due to abundant hot spots, the anisotropic AuCu alloy can significantly enlarge the Raman scattering of MB. Besides, GO is introduced by electrostatic attraction, which further enhances the SERS activity. Moreover, it is found that DNA is able to enhance the SERS activity of AuCu/GO in a sequence and length dual-dependent manner, and short polyT DNA is an effective enhancer. As a result, by a triplex enhancement, Raman signal of MB is greatly increased. To obtain short polyT DNA, APE1-induced cycling amplification is employed. Poly25T-AP containing apurinic/apyrimidinic (AP) site hybridizes with its complementary strand (poly29A) to form double-stranded DNA (dsDNA). In this case, enhancement of SERS activity by DNA is inconspicuous. APE1 is capable to digest the AP site in dsDNA. In the presence of APE1, poly25T-AP is cut at AP site into poly5T-AP that is released from dsDNA. Poly29A can further form another dsDNA and generate more poly5T-AP. The released poly5T-AP is used to enhance SERS signal of MB. Accordingly, concentration of APE1 is quantified by analyzing the SERS response of MB.

First, synthesis of AuNPs is accomplished by the reduction of $HAuCl_4$ with AA in one step. As shown in **Figure 1**a, morphology of the as-prepared AuNPs is spherical. By adding $CuCl_2$ in the process of synthesis, AuCu alloy with a starfish-like structure can be obtained (Figure 1b). Since the obtained AuCu alloy and GO are oppositely charged (Figure S1, Supporting Information), AuCu/GO is further prepared by electrostatic attraction (Figure 1c). Considering that DNA can combine with metallic nanomaterials and GO by base–metal interaction and π–π stacking, respectively, effect of DNA on AuCu/GO is surveyed. The structural information of AuCu/GO/DNA is shown in Figure 1d. The morphology of AuCu/GO/DNA is similar with anisotropic AuCu alloy, and the mean diameter of AuCu/GO/DNA is 55.22 nm (Figure S2, Supporting Information). Meanwhile, typical lattice fringes corresponding to (222) and (111) planar distances of AuCu alloy can be found in AuCu/GO/DNA (Figure 1e,f), indicating AuCu alloy is not affected by the combination with GO and DNA. Besides, several diffraction rings in selected area electron diffraction (SAED) pattern of the AuCu/GO/DNA can be assigned to (110), (200), and (220) planes of AuCu alloy (Figure S3, Supporting Information), suggesting the polycrystalline nature of the AuCu/GO/DNA. The crystal structure of the AuCu alloy is further explored by X-ray diffraction (XRD; Figure S4, Supporting Information): the AuCu alloy has five diffraction peaks at 38.35°, 44.49°, 63.71°, 77.70°, and 81.87°, which are in line with the (111), (200), (220),

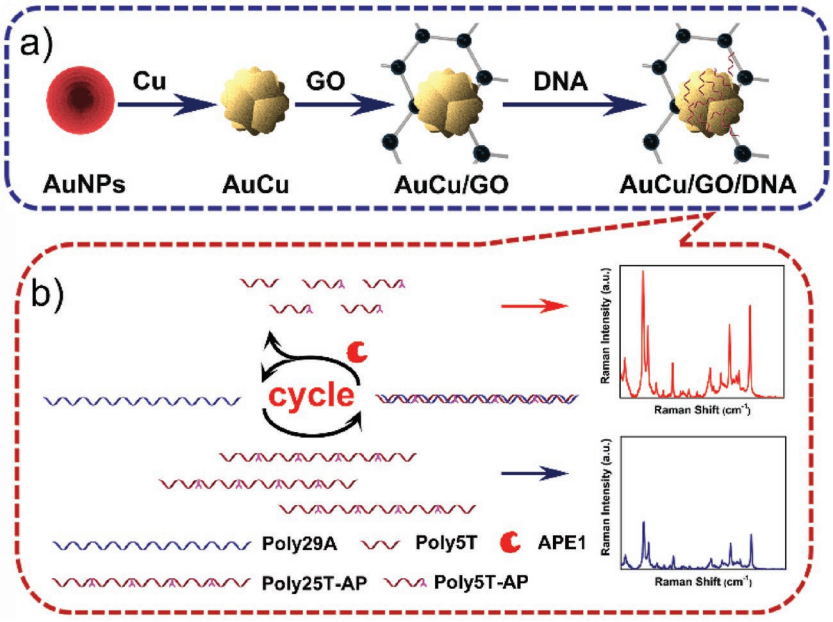

Scheme 1. a) Schematic illustration of the preparation of AuCu/GO/DNA. b) Schematic illustration of an APE1 assay based on GO-assisted and DNA-modulated SERS of AuCu alloy.

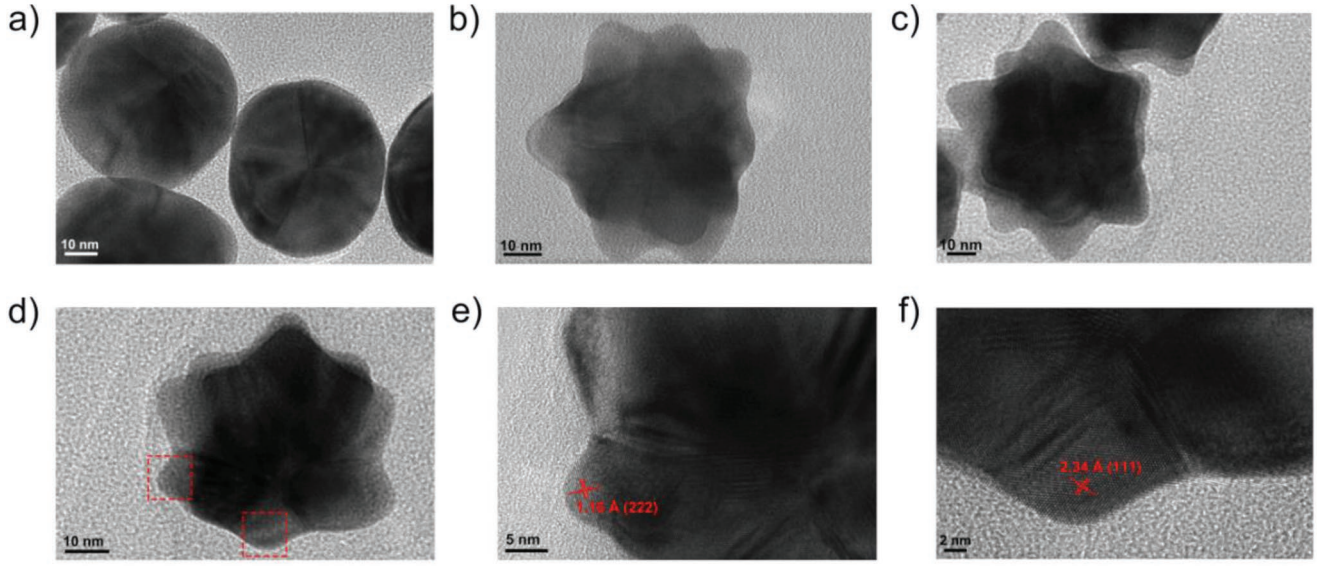

Figure 1. TEM images of a) AuNPs, b) AuCu alloy, c) AuCu/GO, and d) AuCu/GO/DNA. e,f) HRTEM images of the AuCu/GO/DNA from the red-dotted square box in (d).

(311), and (222) reflections (JCPDS 65-2870), respectively. The XRD data match well with that from high-resolution transmission electron microscopy (HRTEM) and SAED.

Elemental distribution of anisotropic AuCu/GO/DNA is investigated by energy dispersive X-ray spectroscopy (EDS) (**Figure 2**). Elementary peaks of Au and Cu can be observed in Figure 2b, suggesting that Au and Cu coexist in the nanomaterial. Besides, according to the data of EDS, molar ratio of Au/Cu is 1.3, which is approximate to feed ratio of $HAuCl_4$ and $CuCl_2$ (1.2). As shown in the EDS line scan (Figure 2c), similar curves of Au and Cu indicate that the starfish-like nanomaterials are AuCu alloy, which is further demonstrated by EDS mapping (Figure 2d–f).

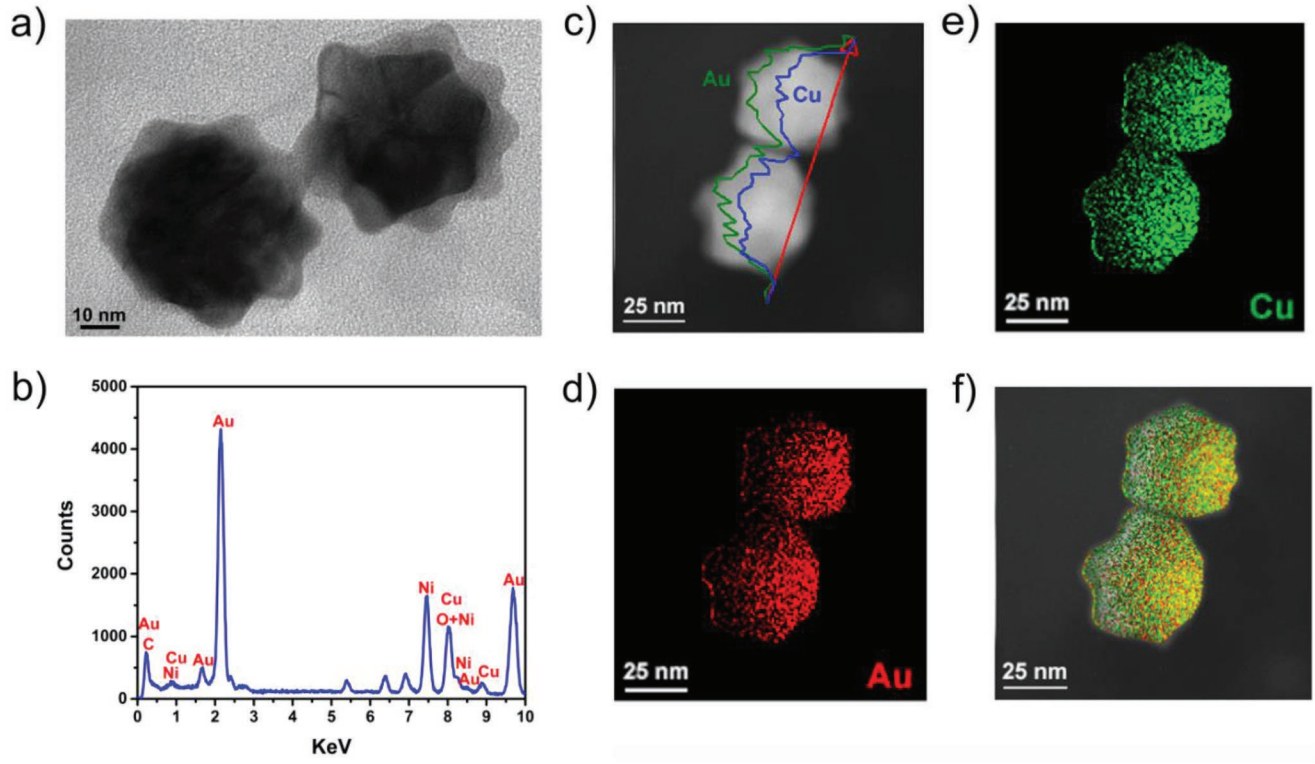

Figure 2. a) TEM image, b) EDS, and c) EDS line profile of AuCu/GO/polyT. d) EDS mapping of Au shown in red. e) EDS mapping of Cu shown in green. f) Mixed EDS mapping of Au and Cu.

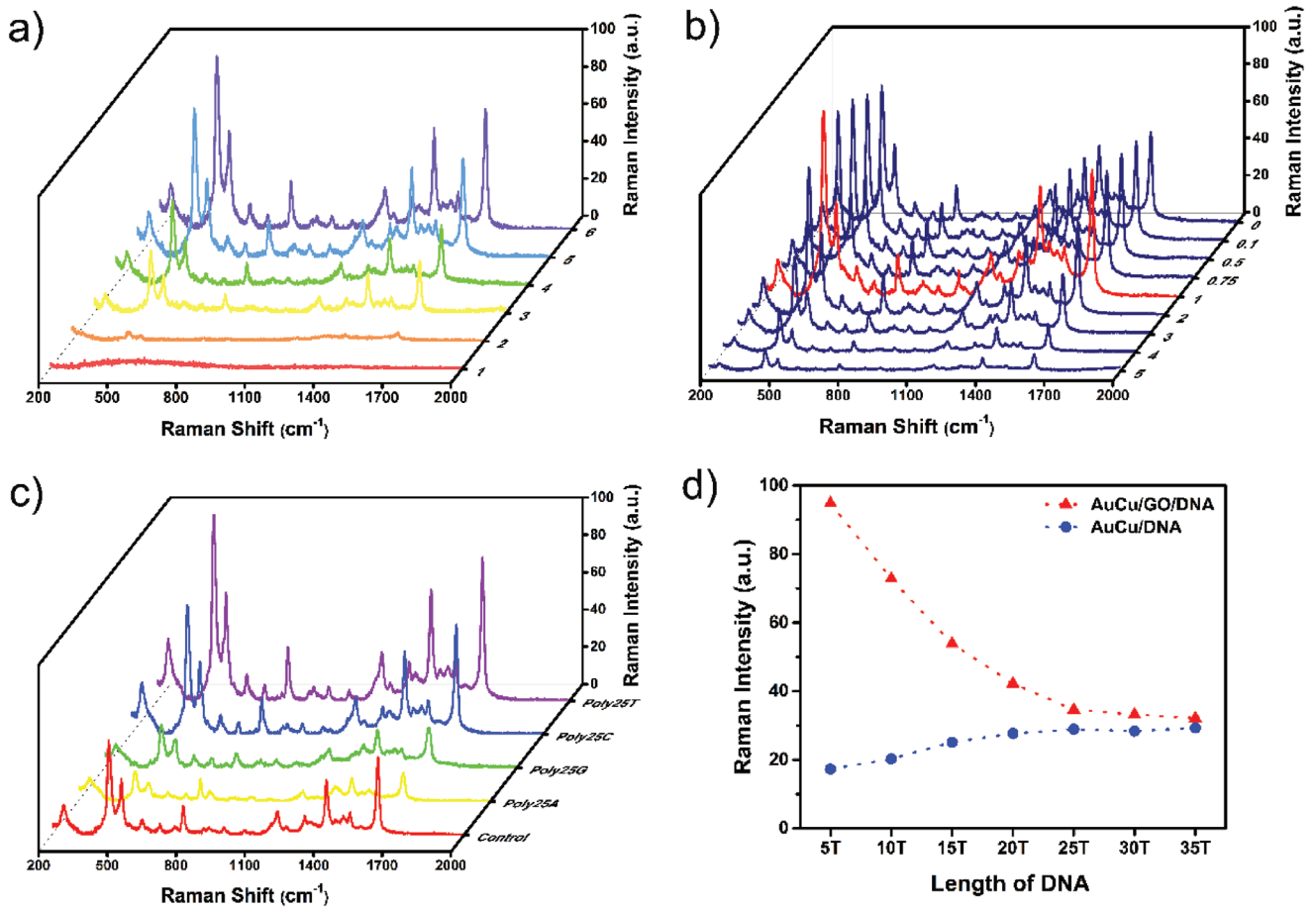

Figure 3. a) SERS spectra of 1) MB, 2) AuNPs/MB, 3) AuCu/MB, 4) AuCu/GO/MB, 5) AuCu/poly25T/MB, and 6) AuCu/GO/poly25T/MB. b) SERS spectra of MB from AuCu/GO/poly25T/MB with different concentrations of GO. c) SERS spectra of AuCu/GO/MB, AuCu/GO/poly25A/MB, AuCu/GO/poly25G/MB, AuCu/GO/poly25C/MB, and AuCu/GO/poly25T/MB. d) Raman intensity of MB at 447 cm^{-1} from AuCu/GO and AuCu with different lengths of DNA.

Figure 3a depicts the enhancement of SERS activity by AuCu alloy, GO, and DNA, respectively. Spherical AuNPs, a common SERS substrate, can slightly improve the SERS signal of MB (curve 2). Since anisotropic structure provides more hot spots, AuCu alloy exhibits higher SERS activity (curve 3). SERS activity is further enhanced by integrating GO into AuCu alloy (curve 4), because GO can cover AuCu alloy and adjust the distribution of AuCu alloy. Besides, GO can induce GERS and absorb more Raman reporters (MB), which may lead to the increase of SERS activity. More interestingly, in comparison with AuCu alloy and AuCu/GO, DNA with a suitable sequence and length can further promote their SERS activities of AuCu/GO (curve 5 and curve 6), suggesting that DNA can be directly used to increase the Raman signal. In addition to AuCu alloy, other alloys including AuAg alloy, AgCu alloy, and AuAgCu alloy are also prepared. As shown in Figure S5 in the Supporting Information, the DNA can only remarkably enhance the SERS activity of AuCu alloy, and other alloys do not have the similar property.

Since effects of GO and DNA on SERS activity depend on the basis of AuCu alloy, the feed ratio of $HAuCl_4$ and $CuCl_2$ is optimized, and 1.2 is chosen as the best feed ratio for the preparation of high SERS active AuCu alloy (Figure S6, Supporting Information). Effect of GO on SERS activity is further investigated (Figure 3b). At low concentration of GO, SERS activity is enhanced with the addition of GO. However, high concentration of GO will greatly depress the SERS activity of AuCu alloy, because the thick layer of GO outside AuCu alloy may block the contact between hot spots and Raman reporters, thus reducing GERS.

As shown in Figure 3c, DNA with different sequences has distinct effects on SERS activity of AuCu/GO. Pyrimidine bases can increase the activity, and the increment of T is larger than that of C. On the contrary, purine bases will decrease the activity, and the decrement of A is larger than that of G. We believe the interactions between bases and metal ions play a key role in regulating SERS activity. It is reported that the adsorption affinity of bases with AuNPs is in an order of T < C < G < A. Besides, polyT has been widely used as template to form Cu nanomaterials for the interaction between T and Cu^{2+}, and polyA is the template of AuNPs.[33] According to our results, enhancement of bases to SERS activity of AuCu/GO is in an order of T > C > G > A. Therefore, it can be concluded that the base apt to bind Cu in AuCu/GO will be an enhancer of SERS activity, while the one

apt to bind Au in AuCu/GO will be a quencher. From the perspective of DNA sequence, polyT is the best choice to increase SERS activity of AuCu/GO.

Besides of sequence, length of DNA can also affect the enhancement of SERS activity. As depicted in Figure 3d, effects of DNA on the SERS activity of AuCu alloy and AuCu/GO are different. Taking AuCu alloy as a substrate, the Raman intensity of MB increases with length of polyT changing from 5T to 25T, and then reaches to a plateau, suggesting that long polyT will benefit from the increase of SERS signal. If AuCu/GO is chosen as a substrate, the Raman intensity of MB is enlarged at any length of polyT, but an opposite trend can be observed. The phenomenon should be ascribed to the π–π stacking between single-stranded DNA and GO. In company with the increase of length, the π–π stacking between polyT and GO becomes stronger. In this case, polyT is apt to be absorbed on the surface of GO rather than AuCu alloy. Therefore, in comparison with short polyT, the enhancement caused by long polyT will be weakened. Basically, effect of DNA on SERS activity of AuCu/GO is sequence and length dual-dependent, and short polyT will maximize the enhancement of SERS activity.

As a multifunctional enzyme, APE1 is crucial to maintain the genome stability.[34] Abnormal levels of APE1 in blood or tissue provide vital information for clinical cancer screening and disease diagnosis.[35] Up to now, a number of approaches have been developed for the detection of APE1,[36] but sensitive methods are still in great lack. Apart from detection method itself, good substrate and cycling amplification strategy are also helpful to improve the sensitivity of our proposed SERS biosensor. First, concentration of MB used in the biosensor is optimized (Figure S7, Supporting Information). The SERS biosensor is fabricated with two DNA, i.e., poly25T-AP and poly29A. In the pursuit of better analytical performance, the ratio of poly25T-AP/poly29A is also studied (**Figure 4**a). By comparing the Raman signal of MB with and without APE1, it can be found that the biggest difference is obtained when the ratio of poly25T-AP/poly29A is 5. The experimental results indicate that poly25T-AP can be digested into short poly5T-AP by APE1, and poly29A is repeatedly used in cycling amplification. Under the optimal conditions, APE1 is quantified using the Raman intensity of MB at 447 cm^{-1} (I_{447}). As shown in Figure 4b, with the increase of APE1, more poly5T-AP is

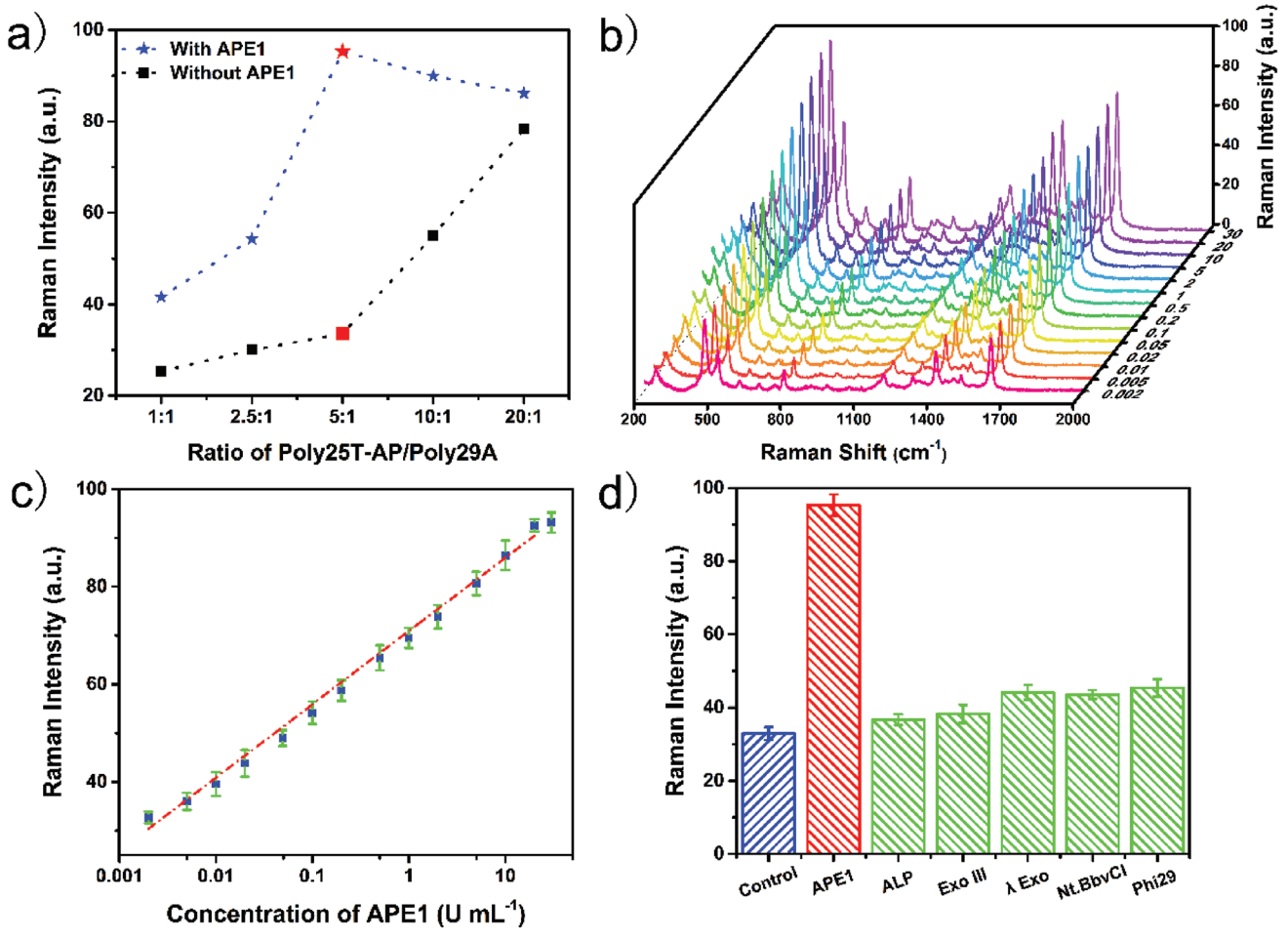

Figure 4. a) Raman intensity of MB at 447 cm^{-1} from AuCu/GO with and without APE1 at different ratios of poly25T-AP and poly29A. The concentration of APE1 used in this assay is 20 U mL^{-1}. b) SERS spectra of MB from AuCu/GO/poly25T in the presence of APE1 with different concentrations from 0.002 to 30 U mL^{-1}. c) Raman intensity of MB at 447 cm^{-1} as a function of the logarithm of APE1 activity. d) Raman intensity of MB at 447 cm^{-1} in the presence of APE1, ALP, Exo III, λ Exo, Nt.BbvCI, and Phi29. The activity of enzymes used in this assay is 1 U.

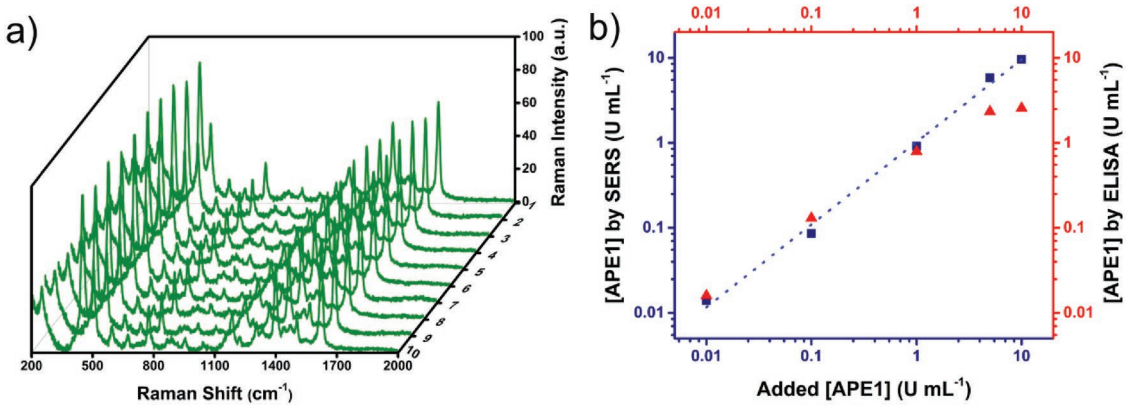

Figure 5. a) SERS spectra of MB in the presence of ten independent samples. b) Results of the SERS biosensor and ELISA for the quantification of APE1 in human serums.

produced and employed to enhance Raman activity of AuCu/GO, thereby leading to the increase of I_{447}. According to the results of Figure 4c, this biosensor exhibits a good linear relationship between the concentration of APE1 ([APE1]) and the I_{447} in a range from 0.002 to 20 U mL^{-1}. The calibration equation is I_{447} = 15.02 log$^{[APE1]}$ + 70.93 (R = 0.996). The calculated detection limit is 0.001 U mL^{-1}, which is better than APE1 biosensors reported before (Table S1, Supporting Information). More importantly, to our knowledge, this is the first APE1 biosensor based on a SERS method.

Selectivity of an analytical approach is of great importance in real sample detection. The selectivity of this APE1 biosensor is evaluated by challenging it with several other enzymes, including alkaline phosphatase (ALP), exonuclease III (Exo III), lambda exonuclease (λ Exo), Nt.BbvCl, and phi29 DNA polymerase (Phi29). Different from APE1, these enzymes cannot trigger the enhancement of Raman intensity (Figure 4d), demonstrating satisfactory selectivity of this biosensor.

Reproducibility is an essential parameter of SERS biosensors. Hence, the reproducibility of this biosensor is verified by testing ten independent samples obtained from parallel assays. As shown in **Figure 5**a, the Raman responses of these samples are similar, and the relative standard deviation of I_{447} is 4.85% (n = 10), implying desirable reproducibility of the proposed biosensor.

To further demonstrate its applicability, the SERS biosensor is employed to quantify APE1 in human serum. The serum samples are diluted 20 times, and spiked with APE1. APE1 in the prepared samples is detected with our method and the standard method (ELISA), respectively. Results of the SERS biosensor reveal a good agreement with the amount of added APE1 (Figure 5b). However, ELISA can only be applied in some of the samples, and false data will be obtained from ELISA if high concentration of APE1 is added to serums. Therefore, in comparison with ELISA, our biosensor is more suitable for practical and clinical applications.

In this work, AuCu alloy with a starfish-like structure is synthesized using a surfactant-free method. The AuCu alloy reveals high SERS activity due to its anisotropic structure that provides plenty of hot spots. To further enhance SERS activity, GO is employed to cover AuCu alloy. In the prepared AuCu/GO, GO acts as a multifunctional SERS enhancer. First, GO can significantly improve the SERS activity by GERS. Second, AuCu alloy is protected by GO, thus promoting the stability of the SERS activity. Third, a large number of Raman reporters, MB, are assembled onto the substrate by GO. Therefore, AuCu/GO can serve as an excellent substrate for SERS investigations. Furthermore, it is found that DNA can directly adjust the SERS activity of AuCu/GO in a sequence and length dual-dependent manner. On the one hand, pyrimidine bases will enhance the activity, while purine bases will depress the activity. On the other hand, short DNA apt to approach AuCu alloy results in larger enhancement of SERS activity than long DNA apt to approach GO. On the basis of this phenomenon, a SERS biosensor is designed by intrinsic effect of DNA on SERS rather than DNA-induced aggregation of metallic nanomaterials. To further improve the performances, APE1-induced cycling amplification is employed in this biosensor, and thus APE1 is sensitively quantified. In addition, the method exhibits satisfactory selectivity and reproducibility. More importantly, the biosensor performs better than standard method for APE1 determination, providing an alternative perspective of fabricating advanced SERS bioanalytical approaches.

Experimental Section

Materials: Gold(III) chloride trihydrate ($HAuCl_4 \cdot 3H_2O$), copper (II) chloride dihydrate ($CuCl_2 \cdot 2H_2O$), silver nitrate ($AgNO_3$), L-ascorbic acid, and methylene blue were obtained from Sigma-Aldrich. Graphene oxide was obtained from Nanjing JCNANO Technology Co., Ltd. (Nanjing, China). Apurinic/apyrimidinic endonuclease 1, lambda exonuclease, Nt.BbvCl, and phi29 DNA polymerase (Phi29) were provided by New England Biolabs (NEB) Ltd. (Beijing, China). Exonuclease III (Exo III) was acquired from Takara Biotechnology Co., Ltd. (Dalian, China). Alkaline phosphatase was provided by Shanghai Sangon Biological Engineering Technology & Services Co., Ltd. (Shanghai, China). The human APE1 enzyme-linked immunosorbent assay kit was obtained from Jiangsu Kejing Biotechnology Co., Ltd. (Yancheng, China). Human serum samples were provided by Jiangsu Cancer Hospital, and used with the approval of the ethical committee of Nanjing Normal University. The above purchased analytical reagents were used as received without any treatments. Ultrapure water (18.2 MΩ cm) from a Milli-Q purification system (Bedford, MA) was utilized in this work.

The DNA used in this work was listed in Table S2 in the Supporting Information. All oligonucleotides were acquired and purified with high-performance liquid chromatography by Shanghai Sangon Biological Engineering Technology & Services Co., Ltd (Shanghai, China).

Instrumentation: The transmission electron microscopy (TEM) images, high-resolution transmission electron microscopy images, energy dispersive X-ray spectroscopy, and selected area electron diffraction analysis were recorded using a JEOL JEM-2100F apparatus at an accelerating voltage of 200 kV. The zeta potential measurements were carried out using a Zetasizer Nano ZS90 Analyzer (Malvern). The X-ray diffraction pattern was obtained using a D/max 2500 VL/PC diffractometer (Japan) equipped with graphite monochromatized Cu Kα radiation (λ = 1.54060 Å) in 2θ ranging from 5° to 90°. The SERS spectra were recorded using a LabRAM HR 800 microspectrometer (Jobin Yvon) with a 785 nm laser excitation source at 100 mW. The collection time of each SERS spectrum was 60 s over a spectral range from 200 to 2000 cm^{-1}.

Synthesis of AuCu/GO and AuCu/GO/DNA: To prepare AuCu/GO, 25 µL of 40×10^{-3} M AA, 50 µL of 1.5×10^{-3} M $HAuCl_4$, and 50 µL of 1.25×10^{-3} M $CuCl_2$ were mixed and incubated at 60 °C for 2 h. Subsequently, 10 µL of 1 mg mL^{-1} GO and 50 µL H_2O were added, followed by keeping the mixture at 60 °C for 1 h. To optimize the feed ratio of $HAuCl_4$ and $CuCl_2$, the concentration of $CuCl_2$ was varied at 0, 0.15, 0.5, 0.75, 1, 1.25, 1.5, 5, and 12×10^{-3} M. To optimize the amount of GO in AuCu/GO, the concentration of GO was varied at 0, 0.1, 0.5, 0.75, 1, 2, 3, 4, and 5 mg mL^{-1}. Before SERS assay, 200 µL of 50×10^{-6} M MB was added into AuCu/GO solution and kept at 60 °C for another 1 h.

To prepare the AuCu/GO/DNA, AuCu alloy was first synthesized as described above. Afterward, 10 µL of 1 mg mL^{-1} GO was added into the solution at 60 °C for 30 min. Then, 50 µL of 2×10^{-6} M DNA (poly25T) solution was added and kept at 60 °C for another 30 min. 50 µL of 2×10^{-6} M poly25A, poly25T, poly25C, and poly25G were chosen to verify the effect of DNA sequence on SERS activity of AuCu/GO. In the case that total amount of thymine remained constant, poly5T, poly10T, poly15T, poly20T, poly25T, poly30T, and poly35T were chosen to verify the effect of DNA length on SERS activity of AuCu/GO. Before SERS assay, 200 µL of 50×10^{-6} M MB was added into AuCu/GO/DNA solution and kept at 60 °C for another 1 h.

Construction of a Novel SERS APE1 Biosensor: First, 10 µL of 10×10^{-6} M poly25T-AP, 10 µL of 2×10^{-6} M poly29A, 5 µL hybridization buffer, and 15 µL H_2O were incubated at 90 °C for 5 min, and then slowly cooled to room temperature. Second, 10 µL of different amounts of APE1 (0.0001, 0.0005, 0.001, 0.005, 0.01, 0.05, 0.1, 0.5, 1, 1.5 U) was added into the mixture and kept at 37 °C for 1 h. Finally, the reacted solution was applied to synthesize AuCu/GO/DNA. To verify the selectivity of this biosensor, 10 µL of other enzymes including APE1, ALP, Exo III, λ Exo, Nt.BbvCl, and Phi29 were chosen instead of APE1. To verify the repeatability of this biosensor, ten independent samples were obtained from parallel assays.

Analysis of the Concentration of APE1 in Real Human Serum: Human serum samples were obtained from volunteers of Jiangsu Cancer Hospital. Specifically, to evaluate the practical applicability of the proposed system, human serum was diluted 20 times and spiked with APE1 at different activities (0.0005, 0.005, 0.05, 0.25, 0.5 U). Then, the concentration of APE1 in serum was quantified with the proposed biosensor and ELISA, respectively.

Supporting Information

Supporting Information is available from the Wiley Online Library or from the author.

Acknowledgements

This work was supported by the National Natural Science Foundation of China for Projects 21625502 and 21505077 and PAPD.

Conflict of Interest

The authors declare no conflict of interest.

Keywords

apurinic/apyrimidinic endonuclease 1, AuCu alloys, DNA, graphene oxide, SERS biosensors

Received: March 22, 2019
Revised: April 17, 2019
Published online:

[1] L. Tao, K. Chen, Z. Chen, C. Cong, C. Qiu, J. Chen, X. Wang, H. Chen, T. Yu, W. Xie, S. Deng, J. B. Xu, *J. Am. Chem. Soc.* **2018**, *140*, 8696.
[2] a) Z. Wang, S. Zong, L. Wu, D. Zhu, Y. Cui, *Chem. Rev.* **2017**, *117*, 7910; b) C. Qi, L.-H. Fu, H. Xu, T.-F. Wang, J. Lin, P. Huang, *Sci. China: Chem.* **2019**, *62*, 162.
[3] a) W. Xi, B. K. Shrestha, A. J. Haes, *Anal. Chem.* **2018**, *90*, 128; b) S. Huang, X. Ling, L. Liang, Y. Song, W. Fang, J. Zhang, J. Kong, V. Meunier, M. S. Dresselhaus, *Nano Lett.* **2015**, *15*, 2892; c) J. Lin, W. Hao, Y. Shang, X. Wang, D. Qiu, G. Ma, C. Chen, S. Li, L. Guo, *Small* **2018**, *14*, 1703274; d) T. Chung, T. Koker, F. Pinaud, *Small* **2016**, *12*, 5891.
[4] J. Reguera, J. Langer, D. Jimenez de Aberasturi, L. M. Liz-Marzan, *Chem. Soc. Rev.* **2017**, *46*, 3866.
[5] a) T. Wagner, A. Nedilko, M. Linn, D. N. Chigrin, G. von Plessen, A. Boker, *Small* **2017**, *13*, 1603054; b) H. Huang, J. H. Wang, W. Jin, P. Li, M. Chen, H. H. Xie, X. F. Yu, H. Wang, Z. Dai, X. Xiao, P. K. Chu, *Small* **2014**, *10*, 4012.
[6] a) T. Jiang, G. Chen, X. Tian, S. Tang, J. Zhou, Y. Feng, H. Chen, *J. Am. Chem. Soc.* **2018**, *140*, 15560; b) C. H. Zhang, J. Zhu, J. J. Li, J. W. Zhao, *ACS Appl. Mater. Interfaces* **2017**, *9*, 17387.
[7] Y. H. Lee, C. L. Lay, W. Shi, H. K. Lee, Y. Yang, S. Li, X. Y. Ling, *Nat. Commun.* **2018**, *9*, 2769.
[8] a) X. Wang, W. Shi, Z. Jin, W. Huang, J. Lin, G. Ma, S. Li, L. Guo, *Angew. Chem.* **2017**, *129*, 9983; *Angew. Chem., Int. Ed.* **2017**, *56*, 9851; b) F. Huang, G. Ma, J. Liu, J. Lin, X. Wang, L. Guo, *Small* **2016**, *12*, 5442.
[9] W. Xi, A. J. Haes, *J. Am. Chem. Soc.* **2019**, *141*, 4034.
[10] H. K. Lee, Y. H. Lee, C. S. L. Koh, G. C. Phan-Quang, X. Han, C. L. Lay, H. Y. F. Sim, Y. C. Kao, Q. An, X. Y. Ling, *Chem. Soc. Rev.* **2019**, *48*, 731.
[11] J. Huang, Y. Zhu, C. Liu, Y. Zhao, Z. Liu, M. N. Hedhili, A. Fratalocchi, Y. Han, *Small* **2015**, *11*, 5214.
[12] H. Kang, J. T. Buchman, R. S. Rodriguez, H. L. Ring, J. He, K. C. Bantz, C. L. Haynes, *Chem. Rev.* **2019**, *119*, 664.
[13] a) K. Liu, Y. Bai, L. Zhang, Z. Yang, Q. Fan, H. Zheng, Y. Yin, C. Gao, *Nano Lett.* **2016**, *16*, 3675; b) B. Paramanik, A. Patra, *J. Mater. Chem. C* **2014**, *2*, 3005; c) T. Zhang, Y. Sun, L. Hang, H. Li, G. Liu, X. Zhang, X. Lyu, W. Cai, Y. Li, *ACS Appl. Mater. Interfaces* **2018**, *10*, 9792.
[14] L. Xue, W. Xie, L. Driessen, K. F. Domke, Y. Wang, S. Schlucker, S. N. Gorb, M. Steinhart, *Small* **2017**, *13*, 1603947.
[15] M. Fan, F.-J. Lai, H.-L. Chou, W.-T. Lu, B.-J. Hwang, A. G. Brolo, *Chem. Sci.* **2013**, *4*, 509.
[16] M. Bańkowska, J. Krajczewski, I. Dzięcielewski, A. Kudelski, J. L. Weyher, *J. Phys. Chem. C* **2016**, *120*, 1841.
[17] a) J. Wu, Y. Xu, P. Xu, Z. Pan, S. Chen, Q. Shen, L. Zhan, Y. Zhang, W. Ni, *Nanoscale* **2015**, *7*, 17529; b) J. Prinz, A. Matkovic, J. Pesic, R. Gajic, I. Bald, *Small* **2016**, *12*, 5458; c) B. Liu, J. Xie, H. Ma, X. Zhang, Y. Pan, J. Lv, H. Ge, N. Ren, H. Su, X. Xie, L. Huang, W. Huang, *Small* **2017**, *13*, 1601001.
[18] a) W. Xu, J. Xiao, Y. Chen, Y. Chen, X. Ling, J. Zhang, *Adv. Mater.* **2013**, *25*, 928; b) D. Dasler, R. A. Schafer, M. B. Minameyer, J. F. Hitzenberger, F. Hauke, T. Drewello, A. Hirsch, *J. Am. Chem. Soc.* **2017**, *139*, 11760.

[19] W. Xu, X. Ling, J. Xiao, M. S. Dresselhaus, J. Kong, H. Xu, Z. Liu, J. Zhang, *Proc. Natl. Acad. Sci. USA* **2012**, *109*, 9281.
[20] S. Panda, T. K. Rout, A. D. Prusty, P. M. Ajayan, S. Nayak, *Adv. Mater.* **2018**, *30*, 1702149.
[21] a) V. Palermo, I. A. Kinloch, S. Ligi, N. M. Pugno, *Adv. Mater.* **2016**, *28*, 6232; b) C. Su, R. Tandiana, J. Balapanuru, W. Tang, K. Pareek, C. T. Nai, T. Hayashi, K. P. Loh, *J. Am. Chem. Soc.* **2015**, *137*, 685.
[22] J. J. Shao, W. Lv, Q. H. Yang, *Adv. Mater.* **2014**, *26*, 5586.
[23] L. Wu, L. Zeng, X. Jiang, *J. Am. Chem. Soc.* **2015**, *137*, 10052.
[24] F. Zeng, D. Xu, C. Zhan, C. Liang, W. Zhao, J. Zhang, H. Feng, X. Ma, *ACS Appl. Nano Mater.* **2018**, *1*, 2748.
[25] a) E. Morales-Narváez, L. Baptista-Pires, A. Zamora-Gálvez, A. Merkoçi, *Adv. Mater.* **2017**, *29*, 1604905; b) F. Bian, J. Wu, H. Wang, L. Sun, C. Shao, Y. Wang, Z. Li, X. Wang, Y. Zhao, *Small* **2018**, *14*, 1803551.
[26] a) J. Su, D. Wang, L. Norbel, J. Shen, Z. Zhao, Y. Dou, T. Peng, J. Shi, S. Mathur, C. Fan, S. Song, *Anal. Chem.* **2017**, *89*, 2531; b) L. Qi, M. Xiao, X. Wang, C. Wang, L. Wang, S. Song, X. Qu, L. Li, J. Shi, H. Pei, *Anal. Chem.* **2017**, *89*, 9850; c) Y. Zhang, Z. Wang, L. Wu, S. Zong, B. Yun, Y. Cui, *Small* **2018**, *14*, 1704433.
[27] J. Guo, Y. Chen, Y. Jiang, H. Ju, *Chem. - Eur. J.* **2017**, *23*, 9332.
[28] a) Y. He, X. Yang, R. Yuan, Y. Chai, *Anal. Chem.* **2017**, *89*, 8538; b) R. Chen, H. Shi, X. Meng, Y. Su, H. Wang, Y. He, *Anal. Chem.* **2019**, *91*, 3597.
[29] B. Liu, P. Wu, Z. Huang, L. Ma, J. Liu, *J. Am. Chem. Soc.* **2018**, *140*, 4499.
[30] a) X. Zhang, Z. Dai, S. Si, X. Zhang, W. Wu, H. Deng, F. Wang, X. Xiao, C. Jiang, *Small* **2017**, *13*, 1603347; b) S. Li, L. Xu, W. Ma, H. Kuang, L. Wang, C. Xu, *Small* **2015**, *11*, 3435; c) X. Ou, X. Lou, F. Xia, *Sci. China: Chem.* **2017**, *60*, 663.
[31] a) D. Lyu, J. Li, X. Wang, W. Guo, E. Wang, *Anal. Chem.* **2019**, *91*, 2050; b) J. Sun, T. Hu, X. Xu, L. Wang, X. Yang, *Nanoscale* **2016**, *8*, 16846.
[32] L. H. Tan, Y. Yue, N. S. Satyavolu, A. S. Ali, Z. Wang, Y. Wu, Y. Lu, *J. Am. Chem. Soc.* **2015**, *137*, 14456.
[33] Z. Y. Li, Y. T. Wu, W. L. Tseng, *ACS Appl. Mater. Interfaces* **2015**, *7*, 23708.
[34] N. A. Moor, I. A. Vasil'eva, R. O. Anarbaev, A. A. Antson, O. I. Lavrik, *Nucleic Acids Res.* **2015**, *43*, 6009.
[35] a) J. Zhai, Y. Liu, S. Huang, S. Fang, M. Zhao, *Nucleic Acids Res.* **2017**, *45*, e45; b) G. Antoniali, F. Serra, L. Lirussi, M. Tanaka, C. D'Ambrosio, S. Zhang, S. Radovic, E. Dalla, Y. Ciani, A. Scaloni, M. Li, S. Piazza, G. Tell, *Nat. Commun.* **2017**, *8*, 797.
[36] a) J. Han, Y. Zhuo, Y. Chai, Y. Xiang, R. Yuan, Y. Yuan, N. Liao, *Biosens. Bioelectron.* **2013**, *41*, 116; b) Y. Zhuo, N. Liao, Y. Q. Chai, G. F. Gui, M. Zhao, J. Han, Y. Xiang, R. Yuan, *Anal. Chem.* **2014**, *86*, 1053.